タイトル Title	Dealkylation of alkyl polycyclic aromatic hydrocarbon over silica monolayer solid acid catalyst
著者 Auther(s)	Katada, Naonobu; Kawaguchi, Yusuke; Takeda, Kazuki; Matsuoka, Taku; Uozumi, Naoki; Kanai, Kazuki; Fujiwara, Shohei; Kinugasa, Keisuke; Nakamura, Koshiro; Suganuma, Satoshi; Nanjo, Masato
掲載誌・巻号・ページ Citation	Applied Catalysis A: General , 530 : 93 - 101
刊行日 Issue Date	2017-01-25
資源タイプ Resource Type	学術雑誌論文 / Journal Article
版区分 Resource Version	著者版 / Author
権利 Rights	© 2016 Elsevier B.V. All rights reserved.
DOI	10.1016/j.apcata.2016.11.018
URL	https://repository.lib.tottori-u.ac.jp/6921

Dealkylation of Alkyl Polycyclic Aromatic Hydrocarbon over Silica Monolayer Solid Acid Catalyst

Naonobu Katada[1]*, Yusuke Kawaguchi[1], Kazuki Takeda[1], Taku Matsuoka[1], Naoki Uozumi[1], Kazuki Kanai[1], Shohei Fujiwara[1], Keisuke Kinugasa[1], Koshiro Nakamura[1], Satoshi Suganuma[2] and Masato Nanjo[1]

1 Department of Chemistry and Biotechnology, Graduate School of Engineering, Tottori University, 4-101 Koyama-cho Minami, Tottori 680-8552, Japan

2 Center for Research on Green Sustainable Chemistry, Faculty of Engineering, Tottori University, 4-101 Koyama-cho Minami, Tottori 680-8552, Japan

* Corresponding author, katada@chem.tottori-u.ac.jp

Abstract

Dealkylation of alkylnaphthalene, as a model of alkyl polycyclic aromatic hydrocarbon compounds in heavy oils, proceeded selectively on a silica monolayer solid acid catalyst. The activity was generated by the deposition of silica on alumina with generation of Brønsted acidity. The activity and Brønsted acid amount showed the maximum where the monolayer covered the surface, indicating that the Brønsted acid site generated on the silica monolayer was the active species. The activity and selectivity on the silica monolayer were high compared to other aluminosilicate catalysts, and high activity was observed even after calcination at 973-1173 K.

Keywords Alkyl polycyclic aromatic hydrocarbons dealkylation, Silica monolayer solid acid catalyst, Vacuum gas oil

Introduction

Among fractions produced by petroleum refinery [1], polycyclic aromatic hydrocarbons such as naphthalene, phenanthrene, pyrene and their derivatives have little usage. In contrast, the C6-10 fraction useful as gasoline has been preferred to contain high concentration of monocyclic aromatic hydrocarbons, mainly BTX [benzene, toluene (methylbenzene) and xylenes (dimethylbenzene isomers)] due to their high octane values [2], whereas the fraction of hydrocarbons larger than C10 applicable to diesel fuel has been demanded to be enriched with alkanes possessing high cetane values [3]. The BTX is also the raw material of some of the polymers produced and consumed in the largest scale [4]. As well as the fluid catalytic cracking (FCC) maximizing the C5-10 hydrocarbons enriched with BTX [5], in these decades, upgrading techniques based on hydrocracking / hydroprocessing have much been advanced [6-9], because suppression of the aromatic contents of gasoline and diesel fuel for the environmental protection has been desired [10-

12] as well as the removal of hetero element (N, S and metals) compounds [13-16], and increase of the demand for diesel fuel [17,18] caused surplus of the aromatic hydrocarbons including BTX in some extent [10, 19]. In the hydrocracking / hydrotreating, the aromatic hydrocarbons are hydrogenated into the compounds with less aromatic rings [9,20-22], as postulated by the direction from the top to the bottom of Figure 1 (A). The cracking makes the smaller molecules from the larger ones [21-23], i.e., from the right to the left. Combining these reactions, the amount of gasoline, naphtha and diesel fractions are relatively increased [9,24].

Nowadays, importance of the carbon dioxide control and decrease of the growing rate of demand for fuels including gasoline and diesel fuel have been recognized, and therefore we can count disadvantages of conventional hydrocracking in very recent or future situation as the following (a)-(d).

(a) It is difficult to increase the yields of BTX and >C10 alkanes only, causing more consumption of the carbon source and finally the carbon dioxide emission to keep the sufficient supply of BTX and >C10 alkanes.

(b) The practical feed of hydrocracking, e.g., LCO (light cycle oil), with low hydrogen / carbon ratio results in serious catalyst deactivation due to coke formation [25]. Remarkable improvement of reaction conditions [26] and catalyst [27,28] to overcome this problem should be mentioned, but it is necessary to consume large amount of hydrogen for the reaction of a heavy carbon source [9,17,25,29], and it can be one factor of carbon dioxide emission through hydrogen production.

(c) Strong hydrogenation conditions give low yield of BTX in naphtha fraction. The short term prediction emphasizes surplus of total aromatic hydrocarbons including BTX [10], but again the increase of BTX yield will be demanded, because it is the raw material of polymers [4], while all of other types of hydrocarbons will become gradually surplus due to the decrease of demand for fuels [30]. Therefore the low yield of BTX must be the problem in near future.

(d) The cracking of hydrogenated intermediates, i.e., alkanes and cycloalkanes, mainly proceeds via dealkylation of alkyl aromatic intermediates formed by hydrogenation-dehydrogenation processes [21,31], and it generally forms too small alkanes (<C5) at high conversion [24].

An alternative can be drawn in Figure 1 (B). It is predicted that dealkylation of alkyl polycyclic aromatic hydrocarbons (hereafter APAH) via carbenium cation is readily catalyzed by Brønsted acid like cracking of cumene (2-phenylpropane) [32,33]. Hydrogenation of the alkene into alkane should be also easy [19] and requires only one H_2 molecule. The formed alkanes and aromatic compounds with no alkyl branches can be separated by such methods as solvent extraction [34] to give the alkanes whose chain lengths are kept, maximizing the possibility for use as the diesel fuel. On the other hand, aromatic compounds without alkyl branch, i.e., benzene, naphthalene, anthracene, phenanthrene and pyrene etc., will be obtained. Benzene is directly a chemical resource

[4]. Partial hydrogenation of polycyclic aromatic ring into tetralin derivative, e.g,, naphthalene into tetralin [12,22,35-37], is possible on such a catalyst as zeolite-supported molybdenum compound [21,24,35,36]. Ring-opening (dealkylation) of tetralin has been known to proceed over the zeolites with relatively large micropores [6,21,22,35,38]. Thus, this alternative process can maximize the amount of benzene derivatives and long chain alkanes with the minimum consumption of hydrogen.

In order to realize it, it is necessary to develop the following processes (A)-(D).

(A) Dealkylation of APAH

(B) Separation of aromatic compounds and alkanes

(C) Partial hydrogenation of naphthalene, anthracene, phenanthrene and pyrene etc.

(D) Ring-opening of tetralin derivatives.

This paper reports an attempt to develop (A).

Dealkylation of a small alkyl aromatic compound such as cumene is known to be an easy reaction catalyzed by a weak Brønsted acid [32,33]. Related reactions, alkylation and transalkylation of alkylbenzene [39-42], dealkylation of long chain alkylbenzene [43] and disproportionation of alkylnaphthalenes [44] have been studied mainly on zeolites. Typical solid acids such as zeolite and amorphous silica-alumina catalyze not only the dealkylation shown by below (1) but also side reactions such (2) and (3), as stated later. In addition, it has been known that the reaction type (2) preferentially occurred compared to (1) in the non-catalytic reaction [45]. We examined the performances of several catalysts to find a catalyst to selectively enhance the reaction rate of desired reaction, dealkylation (1) and successive hydrogenation (4).

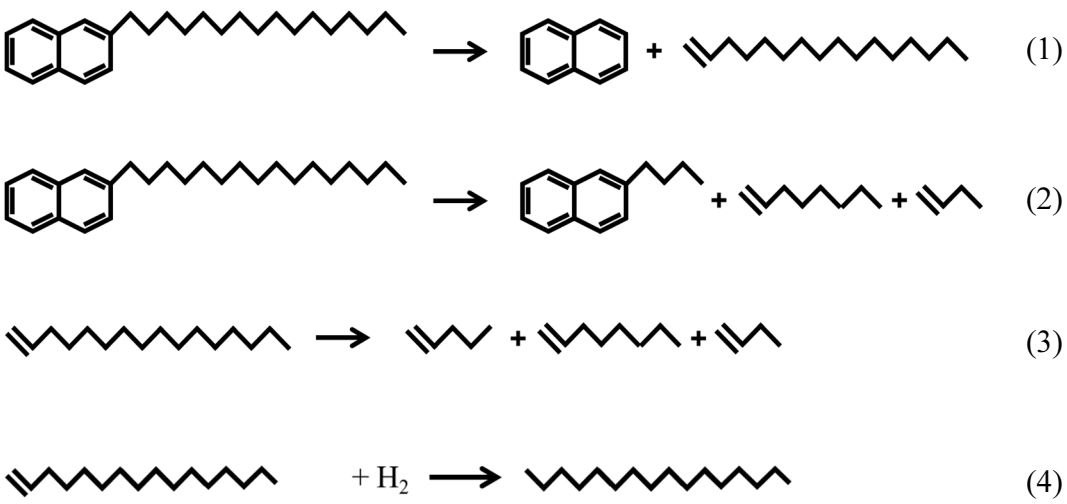

(1)

(2)

(3)

(4)

We here examined aluminosilicates which possessed intrinsically high thermal stability. In order to represent the APAH compounds in typical VGO (Table S2), reagents of alkylnaphthalene was used as model reactants on the first stage of study, and then a practical sample of VGO was examined. In the present study, the components of aromatic and alkyl parts were quantified with an

aid of two-dimensional GC (2D-GC) technique [46,47] which has recently been applied to the analysis of heavy oils [48].

In this study, we examined a silica monolayer loaded on alumina as a candidate of catalyst. Chemical vapor deposition (CVD) of Si precursor on the surfaces of oxides with weakly or moderate basic nature such as alumina and zirconia have been tested to form new catalysts or catalyst supports by several authors [49-58]. Among them, the silica layer on alumina has been found to have catalytic activity for Brønsted acid-catalyzed reactions [50,59] and very high thermal stability [54,57,60]. The influences of precursor of silica, CVD temperature and calculation temperature have been studied extensively as follows. Using tetramethoxysilane [$Si(OCH_3)_4$] at 523-673 K gives a monolayer consisting of a two-dimensional network of Si-O-Si with a small concentration of SiOH, while using $Si(CH_3)_n(OCH_3)_{4-n}$ (n = 1-3) or CVD [61] of tetramethoxysilane at <523 K [62] gives the isolated species. The CVD at >673 K gives heterogeneous thickness of the layer [62]. The Si-O-Al bond was formed during the CVD process, and the remained -OCH_3 group was removed by calcination of the sample at >673 K, as observed by in-situ IR experiments [59] and weight monitoring [62]. The calcination at 673-1173 K gives principally stable properties where the Si concentration was 8-12 nm^{-2} [60]. Based on these facts, we selected tetramethoxysilane as the precursor of silica, 593 K as the CVD temperature and 673 K as the calcination temperature in this study.

In addition, a method of ammonia IRMS (infrared-mass spectroscopy) - TPD (temperature-programmed desorption) was applied to show the acidic property in this study. In this method, absolute quantification of desorbed ammonia is carried out with MS while the temperature dependences of desorption of ammonia from Brønsted and Lewis acid sites are recorded by IR. Combined analysis based on a curve fitting method gives TPD profiles of Brønsted and Lewis acid sites, and then the number and distribution of enthalpy of ammonia desorption as an index of acid strength of each of Brønsted and Lewis acid sites can be obtained [63,64]. In 1990s when the silica monolayer was invented, we had no method for precise measurements of number and strength of each of Brønsted and Lewis acid sites. The discussion was carried out mainly based on the test reactions [62]. In the last decade, we have extensively studied the theory and experimental method of ammonia TPD. This is also the first report of the application of ammonia IRMS-TPD to the silica monolayer.

Experimental

Catalyst preparation

Table 1 shows catalysts employed in this study.

Thin silica layers were prepared by means of a CVD method [59] on alumina JRC-ALO-6,

which had been supplied by Catalysis Society of Japan as a reference catalyst. The deposition was performed in a vacuum system using $Si(OCH_3)_4$ (tetramethoxysilane) as the precursor of silica. After evacuation of the support alumina at 673 K for 2 h, vapor of tetramethoxysilane was admitted to contact with alumina at 593 K, and the resultant increase of weight was monitored using a quartz spring balance. The degree of vacuum was ca. 10^{-3} Torr (1 Torr = 133.3 Pa), and the vapor pressure of alkoxide was kept at ca. 2.5 Torr by chilling the reservoir with an ice bath. After the deposition until the approximately desired weight gain was observed, the sample was calcined in oxygen (200 Torr) at 673 K for >4 h. The amount of deposited Si was calculated from the weight increase with assuming that the formed material was SiO_2.

In addition, three samples of amorphous silica-alumina catalysts industrially available, N631-L (JGC Catalysts and Chemicals Ltd.), reference catalysts JRC-SAH-1 and JRC-SAL-2 (Catalysis Society of Japan, hereafter SAH-1 and SAL-2, respectively) were tested. An Na-Y zeolite 320NAA with FAU structure (Si/Al_2 = 5.9 and [Al] = 4.4 mol kg^{-1}) was supplied by Tosoh Corp., ion-exchanged into NH_4-Y, steamed at 823 K, treated with an NH_4NO_3 aqueous solution at 353 K and dried at 373 K into NH_4-form. It was converted into H-form during the pretreatment of reaction (in-situ preparation). Hereafter it is termed N-USY [65]. Reference catalysts JRC-Z-HB25 (1) with *BEA structure (Si/Al_2 = 25 and [Al] = 1.2 mol kg^{-1}) and JRC-HM20 with MOR structure (Si/Al_2 = 20 and [Al] = 1.5 mol kg^{-1}) distributed by Catalysis Society of Japan were also employed. In addition, a Na-ZSM-5 zeolite HSZ820NAA with MFI structure (Si/Al_2 = 24 and [Al] = 1.3 mol kg^{-1}) was supplied by Tosoh Corp., ion-exchanged with an NH_4NO_3 aqueous solution at 353 K and dried at 373 K into NH_4-form.

Ammonium molybdate [$(NH_4)_6Mo_7O_{24}$] was loaded on alumina JRC-ALO-6 in an aqueous solution with keeping pH at 2 by adding nitric acid, filtered and calcined at 773 K in an oxygen flow to prepare MoO_3/Al_2O_3. The surface concentration of Mo was 5 atoms nm^{-2}, which was determined by ICP-ES (inductively coupled plasma emission spectroscopy, Rigaku CIROS-CCD).

Structural analysis

The nitrogen adsorption isotherm was measured at 77 K using a BELSorp-max equipment (Microtrac-BEL) after pretreatment at 573 K. The surface area was calculated by BET (Brunauer-Emmett-Teller) equation [66], and the pore diameter distribution was analyzed from the desorption branch using a BJH (Barrett-Joyner-Halenda) method [67]. Contribution of the micropore wall to the surface area was evaluated based on a t-plot method [68].

The amount of chemisorbed benzoate anion was measured by a BAT (benzaldehyde-ammonia titration) method [69]. About 40 mg of the sample was packed in a Pyrex tube (4 mm i.d.) and pretreated in a helium flow (27 μmol s^{-1}, atmospheric pressure) at 673 K for 1 h. Benzaldehyde (9.8 μmol) was injected into the sample bed at 523 K in the helium flow, and the eluted aldehyde was

monitored by a GC with a silicone SE-30 packed column and an FID (flame ionization detector). The injection of aldehyde was repeated several times until the saturation of adsorption was observed, and then ammonia (0.41 mmol) was repeatedly supplied at 673 K. The formed benzonitrile was quantified by the GC, and the coverage was calculated on the assumption that the benzoate anion was adsorbed only on the alumina exposed surface but not on the silica-covered surface [59].

The ammonia IRMS-TPD method was applied to measure the number and strength distribution of each of Brønsted and Lewis acid sites [63]. A self-supporting disc (1cm diameter), molded from the sample by compression, was held by a set of metal rings to fix in a cell of Microtrac-BEL IRMS-TPD analyzer and pretreated at 773 K in oxygen. The IR spectra were collected with heating the sample in a helium flow (68 μmol s^{-1}, 6 kPa) at 2 K min^{-1}. Then ammonia was adsorbed at 333 K, and the sample was again heated under the same conditions. The IR spectra and MS response were recorded. The ammonia TPD profile of each of Brønsted and Lewis acid site was analyzed according to our previous study [63]. The number of acid sites was calculated from the peak intensity of the TPD, and the distribution of enthalpy of ammonia desorption (so-called adsorption heat) was analyzed by the curve fitting method [70]. In these experiments, the ammonia adsorption in the ammonia IRMS-TPD analysis was carried out at a relatively low temperature 333 K to keep ammonia on the acid sites with ca. >110 kJ mol^{-1} of the enthalpy of ammonia desorption. We have confirmed that no molecular water was present in these conditions, and that ammonia fully covered the acidic OH groups even in the micropores by the monitoring IR spectrum.

Reaction tests

Dealkylation of cumene (2-phenylpropane) was carried out by means of a pulse method, widely utilized for quick test for solid catalysts, to study the activity for the reaction similar to the target reaction, but the molecular size of reactant was small. The sample was placed in a Pyrex tube (4 mm i.d.). The amount of sample was adjusted to keep the differential conditions (conversion less than 5 %). It was pretreated in a helium flow (41 μmol s^{-1}, atmospheric pressure) at 773 K for 1 h. Cumene (29 μmol) was then injected at 623 K in the helium flow from the septum at the inlet of reactor, and the eluted products were analyzed by a GC connected to the outlet of the reactor. The reaction rate is shown by the amount of consumed cumene divided by the weight of catalyst.

The dealkylation of alkylnaphthalene was carried out as follows. Two types of model reagents of alkylnaphthalene were employed as the reactants. A mixture of hexadecylnaphthalene and octadecylnaphthalene (61 : 39 in molar ratio, consisting of isomer mixture of hexadecylnaphthalene with one alkyl branch whose carbon number was 16 and isomer mixture of octadecylnaphthalene with one alkyl branch whose carbon number was 18) was purchased from Wako Pure Chemical Industries Ltd. Hereafter it is termed C16, 18 AN (alkylnaphthanene) reagent. On the other hand, an isomer mixture of hexadecylnaphthalene with one alkyl branch, whose carbon

number was 16, was purchased from Exxon Mobil Corp. as a commercial sample Synesstic 5. It is termed C16 AN reagent in the following sections.

The schematic diagram of reactor is shown in Figure 2. The catalyst was packed in a stainless steel tube (4 mm i.d.). In typical conditions, the catalyst (solid acid catalyst 50 mg + MoO_3/Al_2O_3 20 mg) was pretreated in a flow of hydrogen (0.12 mol h^{-1}) under atmospheric pressure at 773 K for 1 h. Then, the reactant was fed at 0.96 g h^{-1} with an H_2 flow (0.12 mol h^{-1}) through the catalyst bed at 573 K. In some cases, helium was fed in place of H_2. The total pressure in the tube was kept at 1 MPa using a back pressure valve connected to the outlet. The reaction conditions will be clearly shown by the liquid hourly space velocity (LHSV) defined as [rate of feeding reactant AN (in the standard cases, 0.96 g h^{-1}) / weight of solid acid catalyst employed (in the standard cases, 0.05 g)]. Mesitylene (1,3,5-trimethylbenzene) was fed at g h^{-1} between the catalyst bed and the back pressure valve in order to dissolve and flow solid compounds. The formed material was trapped in a glass tube chilled with an ice bath. The products were analyzed using a 2D-GC (Agilent 7890) with two capillary columns (0.25 μm thickness DB-5MS in length 30 m and i.d. 0.250 mm, and 0.15 μm thickness DB-17HT in length 5 m and i.d. 0.250 mm). An inner standard method was adopted with tetraethylene glycol dimethyl ether as the standard material added after collecting the products. However, mainly because the tailing of GC peaks, the quantification of products contained uncertainties. The components were calculated based on the relative intensities of GC peaks.

Results

Physicochemical properties of catalysts

From the adsorption isotherm of nitrogen at 77 K (examples are seen in Figure S1), the surface area was analyzed based on the BET method [66] (Figure S2). Figure 3 (▲) shows the BET surface area divided by the weight of alumina as a function of the amount of deposited silica, which is shown as the surface concentration (Si atoms nm^{-2}). The change of surface area was little, in consistent with that the silica formed a very thin layer which did not affect the morphology of the particles.

The BAT method showed that the coverage increased with the deposition of silica, as shown in Figure 3 (●). It was in proportion to the amount of silica from 0 to 12 Si nm^{-2}. At 12 Si nm^{-2}, the coverage reached to >90% and kept with further deposition. Because the surface concentration of Al atoms on alumina is believed to be ca. 12 nm^{-2}, it is suggested that the monolayer of silica with 1 : 1 bonding such as Al-O-Si covered almost completely the surface at 12 Si nm^{-2}, as already reported [59].

The surface areas of employed catalysts were summarized as the total surface area in Figure 4. On the other hand, the area of external surface [the surfaces other than the micropore (diameter

< 2 nm) wall, therefore, including the walls of meso- (2 to 50 nm) and macropores (> 50 nm)] was calculated by means of the t-plot analysis (Figure S3) [68]. The difference between the total surface area (BET) and external surface area is assumed to give the area of micropore wall. The area of mesopore wall is estimated by BJH method [67]. As shown in Figure 4, the micropore wall area was negligible on alumina, the silica monolayer loaded on alumina and the amorphous silica-aluminas; the t-plot itself shows the absence of micropore condensation by the adsorption capacity proportional to the estimated thickness of adsorbed material in 0-0.5 nm of the thickness range (Figure S3). On these catalysts, the area of mesopore wall was close to the total surface area, indicating that the mesopores predominantly contributed to form the reaction fields. In contrast, the micropore wall area was close to the total surface area on the zeolites.

The mean pore diameter of alumina-supported silica monolayer was 25 nm, as detemined by the BJH method (Figure 5). The amorphous silica-aluminas had far smaller mesopores in the following order: SAH-1 (6 nm) > SAL-2 (5 nm) > N631-L (4 nm). The pore size distribution in mesopore region of zeolites are overlapped to Figure 5, but the pore size distribution in the micropore region was not able to determine with the BJH analysis assuming Kelvin equation. The small mesopore volumes of employed zeolites are seen in Figure 5, and it is presumed that the micropore wall mainly contributed to the surface area as above. The micropore diameters of zeolites have been known to be <0.8 nm [71], clearly smaller than these values.

The number and strength distribution of Brønsted and Lewis acid sites were analyzed by ammonia IRMS-TPD method, as detailed in Supporting Information. Figure 6 shows that Brønsted acidity was generated by the deposition of silica on alumina. The maximum of number of Brønsted acid site was observed at around 11 Si nm^{-2}, where the monolayer of silica almost completely covered the surface. It suggests that the Brønsted acid site was generated on the monolayer.

The enthalpy of ammonia desorption (so-called adsorption heat) was determined by analysis of the ammonia TPD spectrum to provide a measure of acid strength. We have reported that the enthalpy of Brønsted acid site generated by the framework Al in zeolite had a sharp distribution (shown by an example of MFI in Figure 7) and dependent on the framework type like MOR (150-160 kJ mol^{-1}) > MFI (130-145 kJ mol^{-1}) > *BEA (125-135 kJ mol^{-1}) > FAU (105-115 kJ mol^{-1}) [64,72]. The enthalpy of USY zeolite with FAU structure was however modified by the extra-framework Al species, and that of NH_4NO_3-treated USY (N-USY) was ca. 150 kJ mol^{-1} [65]. Thus various acid strengths were observed on the zeolites. It is believed that the microstructure around the acid site, e.g., interatomic distances and angles, varies the acid strength, and therefore the acid strength was dependent on the framework topology [73]. In contrast, Figure 7 shows broad distributions of ammonia desorption enthalpy on the alumina-supported silica monolayer and the amorphous silica-aluminas. It ranged from 100 to 170 kJ mol^{-1}. It is suggested that the structure

around acid site was widely varied on these materials due to the lack of crystallinity.

Catalytic performance in reactions of AN reagents

Table 2 compares the catalytic activities for the dealkylation of cumene on the alumina-supported silica monolayer and amorphous silica-aluminas. Generally the activity was low on the silica monolayer, and then SAH-1 < SAL-2 < N631-L. It is noteworthy that the activity of zeolite for this reaction was quite high, at least 20 mol g^{-1} on ZSM-5 and Y, and it was impossible to keep the differential conditions and therefore impossible to quantify the reaction rate in the same conditions.

Figure 8 shows a typical example of the time course of the reaction behavior in the dealkylation of alkylnaphthalene using the C16, 18 AN reagent. In these conditions, the dealklylation of alkylnaphthalene into naphthalene and alkenes followed by the hydrogenation of alkenes into alkanes is considered to proceed as shown in Supporting Information. The reaction rate slightly decreased with time on stream, but the extent of deactivation was small in the experimental range. Hereafter, the catalytic performance will be shown by the averaged values of conversion and yield for ca. 3 - 8 h of the time on stream where stable activity and selectivity were observed.

Figure 9 shows the catalytic activity for this reaction as a function of the amount of deposited silica on alumina. The alumina support showed little activity. The activity was created by the deposition of silica and showed the maximum at around 10 Si nm^{-2}, where the monolayer of silica approximately covered the surface. The further deposition decreased the activity. A similar trend was observed in a different set of reaction conditions (Figure S8). Although a mixture of silica layers and MoO_3/Al_2O_3 was employed for the above reactions, it has been found that the role of MoO_3/Al_2O_3 was small (Figure S9). The selectivity on the silica-deposited samples was close to 100 %. The distribution of C16 and 18 among the formed alkanes was also close to 100 %. The selectivity was kept high in 573 - 673 K but decreased at higher temperatures (Figure S10).

Experiments using a practical sample of VGO showed that the reaction was prohibited by basic materials in practical petroleum. After the removal of basic components by treatments with acidic ion exchange resin, the dealkylation of alkylnaphthalene and alkylpyrene proceeded in VGO as shown in Supporting Information.

Figure 10 compares the activities and selectivities of various aluminosilicate solid acid catalysts. Both of the activity and selectivity of amorphous silica-aluminas were slightly lower than those of silica monolayer, resulting in the lower yield of desired products. The yield was in the order of SAH-1 > SAL-2 > N631-L; the difference was small. The zeolite β showed the low selectivity due to the formation of both of alkylnaphthalenes with alkyl groups shorter than C16 and alkanes smaller than C16. The N-USY zeolite showed the high selectivity but low activity. The ZSM-5 zeolite showed little activity and, among the formed alkanes, only alkanes shorter than C16

were detected. The activity for the dealkylation was thus found to be in the order of silica monolayer > SAH-1 > SAL-1 > N631-L > N-USY > β > Y > Mordenite > ZSM-5, as shown by the yield of desired products.

Thermal stability

Figure 11 shows changes in BET surface area and activity for the dealkylation of alkylnaphthalene on the alumina-supported silica monolayer and an amorphous silica-alumina (N631-L) by high temperature calcination. The fresh catalyst was calcined at each temperature and then tested in the reaction, and the reaction rate per unit weight in differential conditions (low conversion) was evaluated here in order to compare the intrinsic activity. The surface area and activity of the silica monolayer were kept constant up to 973 K and gradually decreased at higher temperature. The activity was slightly decreased at 1173 K and still observed at 1173 K. The surface area and activity of amorphous silica-alumina was more quickly decreased in 973-1173 K and completely lost at 1373 K. We have reported that the silica monolayer showed the high surface area and Brønsted acidity (activity for double bond isomerization of 1-butene) after high temperature calcination [60], and that the high thermal stability was due to the low concentration of OH groups [74]. It is predicted that high temperature calcination will be necessary for regeneration of the catalyst deactivated by strong adsorption of heavy compounds in practical processes. The durability of silica monolayer catalyst against the high temperature treatment is thus demonstrated.

Discussion

Comparison of aluminosilicate solid acid catalysts

The catalytic activities for both reactions of cumene and alkylnaphthalene were generated by the deposition of silica on alumina, whereas the pure alumina showed negligible activity. The activity showed the maximum at around 10 Si nm^{-2} where the silica monolayer covered the surface, and further deposition decreased the activity. This was not related with the total acid amount, but the amount of Brønsted acid sites measured by the ammonia IRMS-TPD method well explained these changes. The Brønsted acid amount was negligible on the pure alumina, but increased with the deposition of silica up to ca. 12 Si nm^{-2}. Further deposition decreased the Brønsted acid sites. It indicates that the Brønsted acid site generated on the silica monolayer was the active species for the dealkylation of alkyl aromatic compounds. It should be noted that the textural and porous property of alumina is maintained during the CVD of silica as confirmed by the stable BET surface area (Figure 3) and electron microscopy in our previous paper [75]. It can be concluded that the activity was dependent on the Brønsted acid amount where the textural and porous property was equivalent.

The influence of Brønsted acid strength on the activity for dealkylation of alkylnaphthalene was observed in a few examples. The Brønsted acid strength of N-USY was higher than that of Y

[65], whereas the framework and porous structure were same to give the same steric influence. The N-USY zeolite showed higher activity than Y (Figure 10), suggesting that the relatively stronger Brønsted acid site had higher activity.

However, no clear dependence of the activity on Brønsted acid strength and its distribution was found in comparison of catalytic performances among catalysts with different structures. The activity for the desired reaction, dealkylation of alkylnaphthalene, was roughly in the order of silica monolayer > SAH-1 > SAL-2 > N631-L > zeolites (Figure 10). The Brønsted acid strength of silica monolayer and amorphous silica-alumina showed broad distributions (Figure 7), while the zeolites had different strengths with relatively narrow distributions as stated in the previous section. The activity was not related with the Brønsted acid strength.

The activity on MFI zeolite was obviously low, and therefore the activity for dealkylation of alkylnaphthalene can be shown as silica monolayer > SAH-1 > SAL-2 > N631-L > zeolites with 12-rings (FAU, *BEA and MOR) > zeolite with 10-ring (MFI) (Figure 10). This was in agreement with the order of pore size. It is suggested that the steric hindrance was predominant in the kinetics of this reaction, and the silica monolayer showed the relatively high activity because of its large pore size; as the pore diameter of silica monolayer was 25 nm (Figure 5), far larger than the related molecules, and therefore it is perhaps better to say that the present silica monolayer catalyst had non-porous structure resulting in the high activity.

In conclusion, the activity for dealkylation of alkylnaphthalene was sensitive to the pore size rather than the acid strength. The dealkylation of alkyl aromatic hydrocarbon can be catalyzed even by a weak Brønsted acid [32,33]. In the present study, it was indicated that the presence of Brønsted acid site was necessary. However, it was shown that the influence of pore size was predominant compared to the acidic property, presumably because the molecular size of reactant was large. On some of the amorphous silica-aluminas and zeolites, the by-products, i.e., alkylnaphthalenes with shorter alkyl chains and shorter alkanes, were detected. It implies that, in the narrow pores, the cracking of linear alkyl part proceeded readily compared to the reaction of dealkylation of the same molecule, probably due to the poor accessibility of the base of alkyl branch attaching to the aromatic ring.

The activity for the dealkylation of smaller molecule, cumene, was roughly in the reverse order of the activity of the large molecule, alkylnaphthalene (Table 2). It has not been possible to show what controlled the activity of cumene cracking, one can say at least that the activity for dealkylation of bulky molecule is not related with the activity for the same kind of reaction of smaller molecule. It supports that the activity for the reaction of large alkyl aromatic compound was strongly dependent on the accessibility of molecules.

As shown in the previous section, the followings should be studied for maximizing the yield

of monocyclic aromatic compounds, mainly BTX, as well as maximizing the possibility for use of alkyl parts as the diesel fuel.

(A) Dealkylation of APAH

(B) Separation of aromatic compounds and alkanes

(C) Partial hydrogenation of naphthalene, anthracene, phenanthrene and pyrene etc.

(D) Ring-opening of tetralin derivatives.

The present paper demonstrates the possibility of part (A). Besides, (B) - (D) should be also investigated. Among them, the partial hydrogenation (C) [21,24,35,36] and the ring-opening (D) [6,21,22,35,38] have been studied to find suitable catalysts. The present results will be united to these studies to open a way for efficient use of heavy hydrocarbons.

Conclusions

A silica monolayer catalyst was prepared by CVD of tetramethoxysilane on alumina. It showed Brønsted acidity and thermal stability. The silica monolayer showed high activity and selectivity for dealkylation of C16, 18 alkylnaphthalene into naphthalene and C16, 18 alkanes. Among aluminosilicates (silica monolayer, amorphous silica-alumina and zeolites), the activity and selectivity of the silica monolayer were relatively high. The activity was observed even after calcination at 973-1173 K. It is suggested that the silica monolayer catalyst had non-porous structure (pore diameter ca. 25 nm) resulting in the high activity. Tests for application to VGO were carried out, showing potential of the silica monolayer catalyst for dealkylation of alkyl polycyclic aromatic hydrocarbons in heavy oils. Future studies are expected to open a way to unite the dealkylation of alkyl polycyclic aromatic hydrocarbons with separation of aromatic compounds and alkanes, partial hydrogenation of polycyclic aromatics into tetralin derivatives, and ring-opening of tetralin derivatives into benzene derivatives, in order to maximize the yield of monocyclic aromatic compounds, i.e., benzene, toluene and xylene, and to maximize the possibility for use of alkyl parts as the diesel fuel.

Acknowledgement

A part of this work was carried out as a part of Research on Technologies for Advanced Use of Heavy Oil trusted by Ministry of Economy, Trade and Industry, Japan to Japan Petroleum Energy Center. The other part was supported by JSPS KAKENHI Grant Number 16H04568.

---

[1] R.A. Meyers, Handbook of Petroleum Refining Processes, Fourth Edition, McGraw-Hill Education, New York (2016).

[2] American Society of Testing Materials, Knocking Characteristics of Pure Hydrocarbons, ASTM

Special Technical Publication No. 225 (1958).
[3] R. Kakizaki, M. Suzuki, T. Li, H. Ogawa, M. Murase, Trans. Soc. Automotive Engineers Jpn. 40 (2009) 1503-1508.
[4] M. Bender, Abstracts of DGMK International Conference, 2013, German Society for Petroleum and Coal, Science and Technology, Berlin (2013) 59-64.
[5] R. Sadeghbeigi, Fluid Catalytic Cracking Handbook, Third Edition, Elsevier, Amsterdam (2012).
[6] S.C. Korre, M.T. Klein, R.J. Quann, Ind. Eng. Chem. Res. 36 (1997) 2041-2050.
[7] W.-C. Cheng, G. Kim, A.W. Peters, X. Zhao, K. Rajagopalan, Catal. Rev.-Sci. Eng., 40 (1998) 39-79.
[8] C. Song, X. Ma, Appl. Catal., B: Environ. 41 (2003) 207-238.
[9] M.S. Rana, V. Sámano, J. Ancheyta, J.A.I. Diaz, Fuel 86 (2007) 1216-1231.
[10] J. Weitkamp, A. Raichle, Y. Traa, Appl. Catal., A: Gen. 222 (2001) 277-297.
[11] A. Raichle, Y. Traa, J. Weitkamp, Chem. Ing. Tech. 73 (2001) 947-956.
[12] X. Dupain, E.D. Gamas, R. Madon, C.P. Kelkar, M. Makkee, J.A. Moulijn, Fuel 82 (2003) 1559-1569.
[13] W.L. Orr, J.S.S. Damste, ACS Symp. Ser. 429 (1990) 2-29.
[14] G.S. Waldo, R.M.K. Carlson, J.M. Moldowan, K.E.Peters, J.E. Penner-Hahn, Geochim. Cosmochim. Acta, 55 (1991) 801-814.
[15] S. Mitra-Kirtley, O.C. Mullins, J.V. Elp., S.J. George, J. Chen., S.P. Cramer, J. Am. Chem. Soc. 115 (1993) 252-258.
[16] Q.Shi, D. Hou, K.H. Chung, C. Xu, S. Zhao, Y. Zhang, Energy & Fuels, 24 (2010) 2545-2553.
[17] M. Absi-Halabi, A. Stanislaus, D.L. Trimm, Appl. Catal. 72 (1991) 193-215.
[18] A.B. Amara, R. Dauphin, H. Babiker, Y. Viollet, J. Chang, N. Jeuland, A. Amer, Fuel 174 (2016) 63-75.
[19] P. Castaño, A.G. Gayubo, B. Pawelec, J.L.G. Fierro, J.M. Arandes, Chem. Eng. J. 140 (2008) 287-295.
[20] C. Song, Catal. Today, 86 (2005) 211-263.
[21] J. Weitkamp, ChemCatChem 4 (2012) 292-306.
[22] R. Pujro, M. Farco, U. Sedran, J. Chem. Technol. Biotechnol. 91 (2016) 336-345.
[23] X. Dupain, E.D. Gamas, R. Madon, C.P. Kelkar, M. Makkee, J.A. Moulijn, Fuel 82 (2003) 1559-1569.
[24] J. Ancheyta, S. Sánchez, M.A. Rodríguez, Catal. Today 109 (2005) 76-92.
[25] P. Castaño, A. Gutiérrez, I. Hita, J.M. Arandes, A.T. Aguayo, J. Bilbao, Energy & Fuels 26 (2012) 1509-1519.
[26] A. Gutiérrez, J.M. Arandes, P. Castaño, M. Olazar, A. Barona, J. Bilbao, Fuel Proc. Technol. 95

(2012) 8-15.
[27] A. Gutiérrez, J.M. Arandes, P. Castaño, A.T. Aguayo, J. Bilbao, Energy & Fuels 25 (2011) 3389-3399.
[28] A. Gutiérrez, J.M. Arandes, P. Castaño, M. Olazar, J. Bilbao, Fuel Proc. Technol., 101, 2012, 64-72 (2012).
[29] I. Gawel, D. Bociarska, P. Biskupski, Appl. Catal., A: Gen. 295 (2005) 89-94.
[30] T. Nakanishi, R. Komiyama, Supply and Demand Analysis on Pertoleum Products and Crude Oils for Asia and the World, Inst. Energy Economy Jpn. (2006).
[31] B. Sirjean, P.A. Glaude, M.F. Ruiz-Lopez, R. Fournet, J. Phys. Chem., A 110 (2006) 12693-12704.
[32] A. Corma, B.W. Wojciechowski, Catal. Rev. Sci. Eng. 24 (1982) 1-65.
[33] A.M. Youssef, A.I. Ahmed, S.E. Samra, Mater. Lett. 10 (1990) 175-180.
[34] G.W. Cassell, N. Dural, A.L. Hines, Ind. Eng. Chem. Res. 28 (1989) 1369-1374.
[35] S.J. Ardakani, K.J. Smith, Appl. Catal. A: Gen. 403 (2011) 36-47.
[36] T. Choi, J. Lee, J. Shin, S. Lee, D. Kim, J.K. Lee, Appl. Catal. A: Gen. 492 (2015) 140-150.
[37] P. Castaño, J.M. Arandes, M. Olazar, J. Bilbao, B. Pawelec, U. Sedrán, Catal. Today 150 (2010) 363-367.
[38] R. Contreras, J. Ramírez, R. Cuevas-Carcía, A. Gutiérrez-Alejandre, P. Castillo-Villalón, G. Macías, I. Puente-Lee, Catal. Today 148 (2009) 49-54.
[39] J.L. Hodala, A.B. Halgeri, G.V. Shanbhag, Appl. Catal. A: Gen. 484 (2014) 8-16.
[40] H. Liu, G. Yang., React. Kinet. Mech. Catal. 113 (2014) 605-614.
[41] S.A. Ali, A.M. Aitani, J. Čejka, S.S. Al-Khattaf, Catal. Today 243 (2015) 118-127.
[42] C. Hu, J. Li, W. Jia, M. Liu, Z. Hao, Z. Zhu, Chin. J. Chem. 33 (2015) 247-252.
[43] A.L. Petre, W.F. Hoelderich, M.L. Gorbaty, Appl. Catal. A: Gen. 363 (2009) 100-108.
[44] R. Brzowski, W. Skupiński, J. Catal. 220 (2003) 13-22.
[45] C.M. Smith, P.E. Savage, Ind. Eng. Chem. Res. 30 (1991) 331-339.
[46] J. Beens, U.A.T. Brinkman, Anal. Biochem. Chem. 378 (2004) 1939-1943.
[47] T. Górecki, J. Harynuk, O. Panić, J. Sep. Sci. 27 (2004) 359-379.
[48] J.H. Marsman, J. Wildschut, F. Mahfud, H.J. Heeres, J. Chromatogr., A 1150 (2007) 21-27.
[49] T. Jin, T. Okuhara, J.M. White, J. Chem. Soc., Chem. Commun. (1987) 1248-1249.
[50] S. Sato, M. Toita, Y.-Q. Yu, T. Sodesawa, F. Nozaki, Chem. Lett. (1987) 1535-1536.
[51] M. Niwa, T. Hibino, H. Murata, N. Katada, Y. Murakami, J. Chem. Soc., Chem. Commun. (1989) 289 - 290.
[52] B.-Q. Xu, T. Yamaguchi, K. Tanabe, Chem. Lett. (1989) 149-152.
[53] H. Fukui, T. Ogawa, M. Nakano, M. Yamaguchi, Y. Kanda, in Controlled Interphases in

Composite Materials, ed. by H. Ishida, Springer, Berlin (1990) 469-478.
[54] B. Beguin, E. Grabowski, M. Primet, J. Catal. 127 (1991) 595-604.
[55] N. Okazaki, T. Kohno, R. Inoue, Y. Imizu, A. Tada, Chem. Lett. (1993) 1195-1198.
[56] P. Sarrazin, S. Kasztelan, N. Zanier-Szyndlowski, J.P. Bonnelle, J. Grimblot, J. Phys. Chem. 97 (1993) 5947-5953.
[57] T. Horiuchi, T. Sugiyama, T. Mori, J. Mater. Chem. 3 (1993) 861-865.
[58] T.-C. Sheng, I.D. Gay, J. Catal. 145 (1994) 10-15.
[59] M. Niwa, N. Katada, Y. Murakami, J. Phys. Chem. 94 (1990) 6441-6445.
[60] N. Katada, H. Ishiguro, K. Muto, M. Niwa, Adv. Mater. Chem. Vap. Deposition 1 (1995) 54-60.
[61] N. Katada, T. Tsubouchi, T. Toyama, M. Niwa, Y. Murakami, Res. Chem. Intermed., 9 (1995) 137-149.
[62] N. Katada, T. Toyama, M. Niwa, J. Phys. Chem., 98 (1994) 7647-7652.
[63] M. Niwa, K. Suzuki, N. Katada, T. Kanougi, T. Atoguchi, J. Phys. Chem. B 109 (2005) 18749-18757.
[64] M. Niwa, N. Katada, K. Okumura, Characterization and Design of Zeolite Catalysts: Solid Acidity, Shape Selectivity and Loading Properties, Springer, Berlin, Heidelberg, Dordrecht and New York (2010).
[65] K. Okumura, T. Tomiyama, N. Morishita, T. Sanada, K. Kamiguchi, N. Katada, M. Niwa, Appl. Catal. A: Gen. 405 (2011) 8-17.
[66] S. Brunauer, P.H. Emmett, E. Teller, J. Am. Chem. Soc. 60 (1938) 309-319.
[67] E.P. Barrett, L.G. Joyner, P.P. Halenda, J. Am. Chem. Soc. 73 (1951) 373-380.
[68] A. Galarneau, F. Villemot, J. Rodriguez, F. Fajula, B. Coasne, Langmuir 30 (2014) 13266-13274.
[69] M. Niwa, S. Inagaki, Y. Murakami, J. Phys. Chem. 89 (1985) 3869-3872.
[70] N. Katada, T. Tsubaki, M. Niwa, Appl. Catal. A: Gen. 340 (2008) 76-86.
[71] D.W. Breck, Zeolite Molecular Sieves: Structure, Chemistry and Use, John Wiley and Sons, New York (1974).
[72] N. Katada, M. Niwa, Catal. Surveys Asia 8 (2004) 161-170.
[73] N. Katada, K. Suzuki, T. Noda, G. Sastre, M. Niwa, J. Phys. Chem. C 113 (2008) 19208-19217.
[74] N. Katada, T. Fujii, K. Iwata, Y. Hibino, M. Niwa, J. Catal. 186 (1999) 478-480.
[75] K. Muto, N. Katada, M. Niwa, Catal. Today 35 (1997) 145-151.

Table 1 Employed catalysts and their properties

Notation	Description	Composition	Number of Brønsted acid sites / mol kg^{-1}	Number of Lewis acid sites / mol kg^{-1}
MA	MoO_3 loaded on JRC-ALO-6*	Surface concentration of Si atom = 5 nm^{-2}	-	-
Alumina	JRC-ALO-6*	γ-Al_2O_3	0.02	0.22
SA*n*	Alumina-supported silica layer	Surface concentration of Si atom = *n* nm^{-2}	0.29 (SA11)	0.10 (SA11)
N631-L	Amorphous silica-alumina N631-L**	Al_2O_3 13 wt%, SiO_2 87 wt%	0.17	0.11
SAL-2	Amorphous silica-alumina JRC-SAL-2*	Al_2O_3 14 wt%, SiO_2 86 wt%	0.32	0.13
SAH-1	Amorphous silica-alumina JRC-SAH-1*	Al_2O_3 29 wt%, SiO_2 71 wt%	0.32	0.17
Y	In-situ H-form*** of Y zeolite, FAU structure	SiO_2/Al_2O_3 = 5.9	-	-
N-USY	In-situ H-form*** of the steamed and NH_4NO_3-treated USY zeolite, FAU structure		0.51	0.20
β	H-form of Zeolite β, *BEA structure, JRC-Z-HB25 (1)*	SiO_2/Al_2O_3 = 25	0.46	0.06
Mordenite	H-form of mordenite, MOR structure, JRC-Z-HM20*	SiO_2/Al_2O_3 = 20	0.84	0.00
ZSM-5	In-situ H-form*** of ZSM-5 zeolite, MFI structure	SiO_2/Al_2O_3 = 24	1.15	0.00

* Reference catalyst supplied by Reference Catalyst Division, Catalysis Society of Japan.

** Kindly supplied by JGC Catalysts and Chemicals Ltd.

*** The NH_4-form was packed into the reactor and treated in a hydrogen flow at 773 K where the NH_4-form had been confirmed to be converted into the H-form.

Table 2 Catalytic activity for dealkylation of cumene

Catalyst	Reaction rate / mol_{cumeme} kg_{cat}^{-1}
Alumina	0.0003
SA12	0.055
N631-L	1.60
SAL-2	0.933
SAH-1	0.157

Figure captions

Figure 1 Schematic drawing of conventional hydrocracking (A) and dealkylation followed by partial hydrogenation of polyaromatics (B) of alkylaromatic hydrocarbons.

Figure 2 Schematic drawing of reactor for dealkylation of alkylnaphthalene. 1: Mass flow control valve, 2: Pressure gauge, 3: Thermocouple, 4: Pump for high pressure liquid chromatography, 5: Capillary for stabilization of flow rate, 6: Electric furnace, 7: Glass wool, 8: Back pressure valve, 9: Ice bath.

Figure 3 Plots of BET surface area divided by weight of alumina (▲) and coverage (●) on silica-deposited alumina.

Figure 4 Areas of total surface (), external surface (), micropore wall () and mesopore wall () analyzed from nitrogen adsorption isotherm at 77 K. The analytical method is shown in Supporting Information.

Figure 5 Mesopore size distributions of alumina-supported silica monolayer (SA12,), SAH-1 (), SAL-2 (), N631-L (), Y (), N-USY (), β (), mordenite ()and ZSM-5 () detemined by BJH method.

Figure 6 Number of Brønsted (●) and Lewis (■) acid sites on silica-deposited alumina determined by ammonia IRMS-TPD method. The TPD profile (plots of concentration of ammonia in the gas phase against the temperature) was recorded by a MS (mass spectrometer). It was deconvoluted into the factions ascribed to Brønsted and Lewis acid sites based on the temperature dependences of intensities of species adsorbed on Brønsted and Lewis acid sites in the IR (infrared) spectra. The number of acid sites (= number of ammonia molecules) was calculated by integral of the peak intensity of thus determined TPD profile [63], as detailed in Supporting Information.

Figure 7 Distributions of Brønsted acid strength (enthalpy of ammonia desorption) of silica monolayer (SA11,), SAH-1 (), SAL-2 (), N631-L () and ZSM-5 () estimated from shape of ammonia desorption profile of Brønsted acid sites as detailed in Supporting Information.

Figure 8 Time course of activity (conversion, ●) and selectivity (△) on SA8 for dealkylation of

C16, 18 AN reagent at 573 K and LHSV = 19 $g_{\text{-C16, 18 AN}}$ $g_{\text{-SA8}}^{-1}$ h^{-1} in co-presence of MA (solid acid : MA weight ratio = 5 : 2).

Figure 9　Plots of conversion (●), selectivity (△) and distribution of C16-18 alkanes in formed alkanes (▽) in dealkylation of C16, 18 AN reagent at 573 K and LHSV = 15 $g_{\text{-C16, 18 AN}}$ $g_{\text{-SA}}^{-1}$ h^{-1} in co-presence of MA (solid acid : MA weight ratio = 5 : 2) against amount of deposited silica on alumina.

Figure 10　Conversion (■), yield of desired products (□), selectivity (■) and distribution of C16-18 alkanes in formed alkanes (■) in dealkylation of C16, 18 AN reagent at 573 K and LHSV = 15 $kg_{\text{C16, 18 AN}}$ kg_{cat}^{-1} h^{-1} in co-presence of MA (solid acid : MA weight ratio = 5 : 2) on various catalysts.

Figure 11　BET surface area (▲ and △) and reaction rate measured with adjusting catalyst amount to keep low conversion (< 17%) in dealkylation of C16 AN reagent (feed rate = 0.097 $g_{\text{-C16 AN}}$ h^{-1}) at 673 K (● and ○) on 15.5 wt% silica-deposited alumina (▲ and ●, SA10) and amorphous silica-alumina N631-L (△ and ○) calcined at various temperatures.

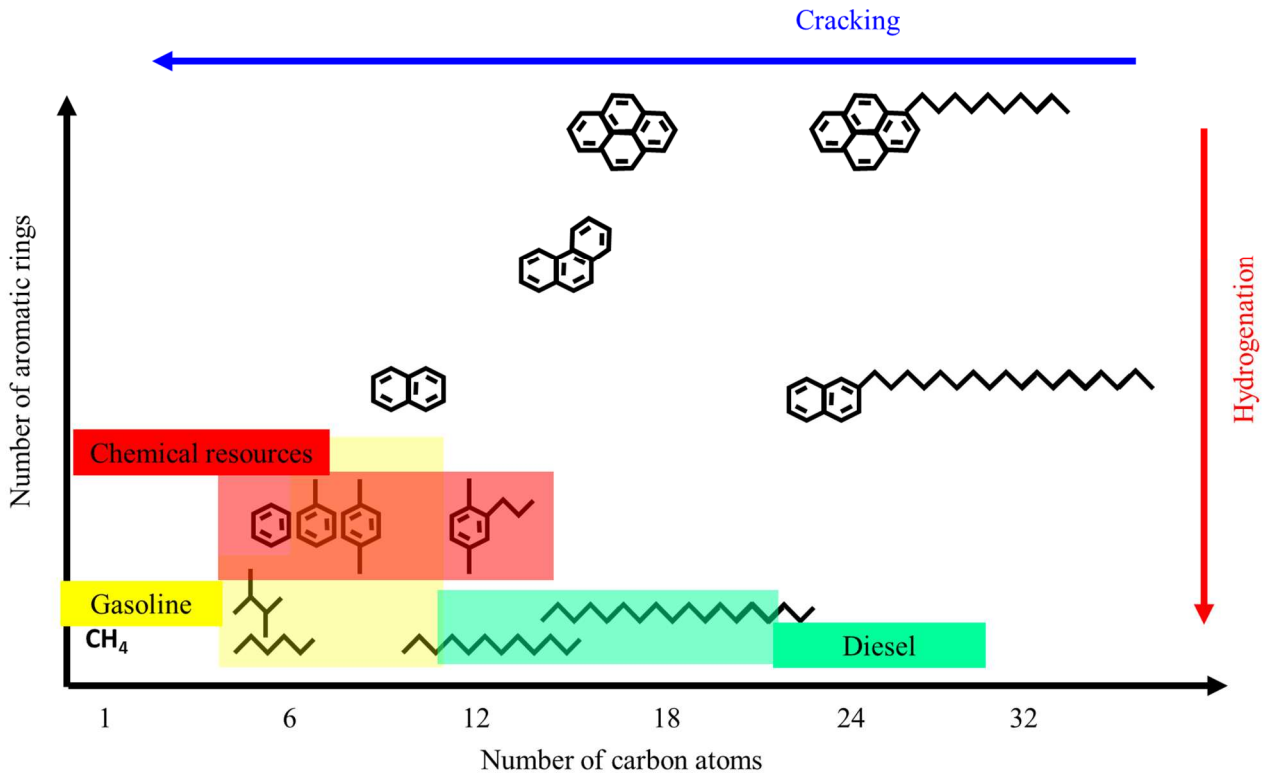
Cracking
Hydrogenation
Number of aromatic rings
Chemical resources
Gasoline
CH4
Diesel
1
6
12
18
24
32
Number of carbon atoms

Figure 1 (A)

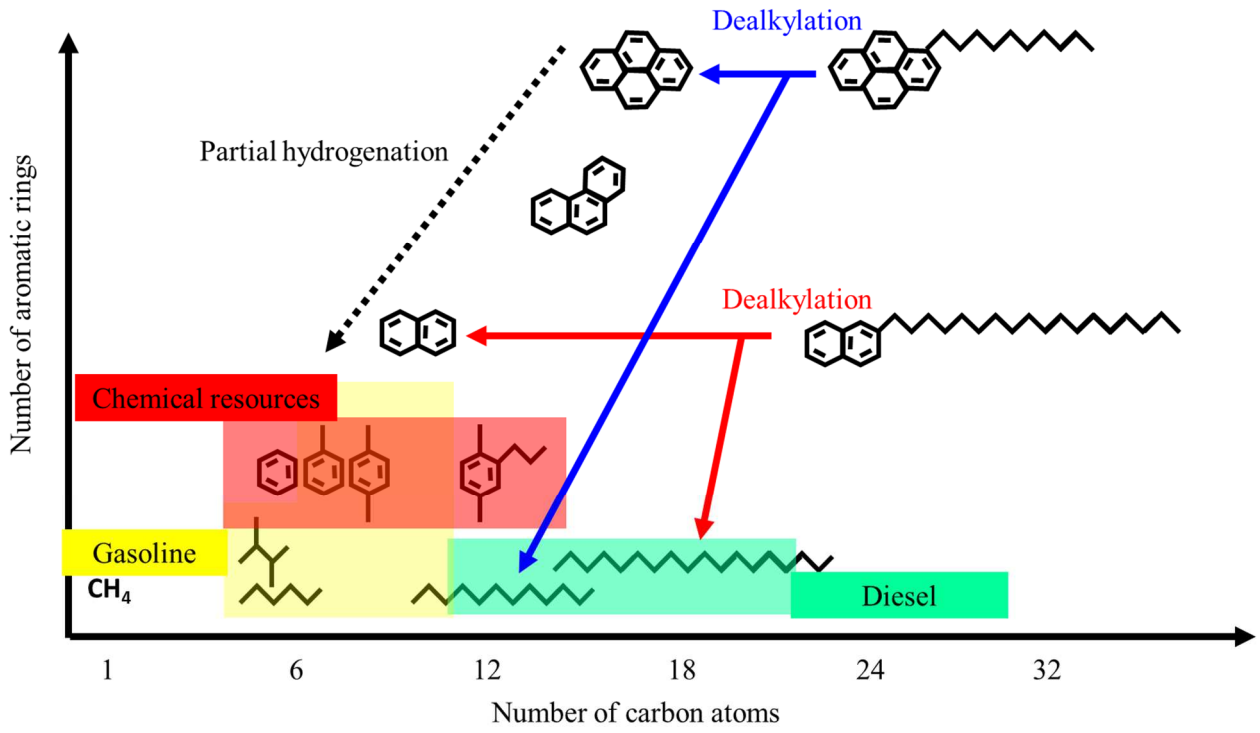
Dealkylation
Partial hydrogenation
Dealkylation
Chemical resources
Gasoline
CH4
Diesel
Number of aromatic rings
1
6
12
18
24
32
Number of carbon atoms

Figure 1 (B)

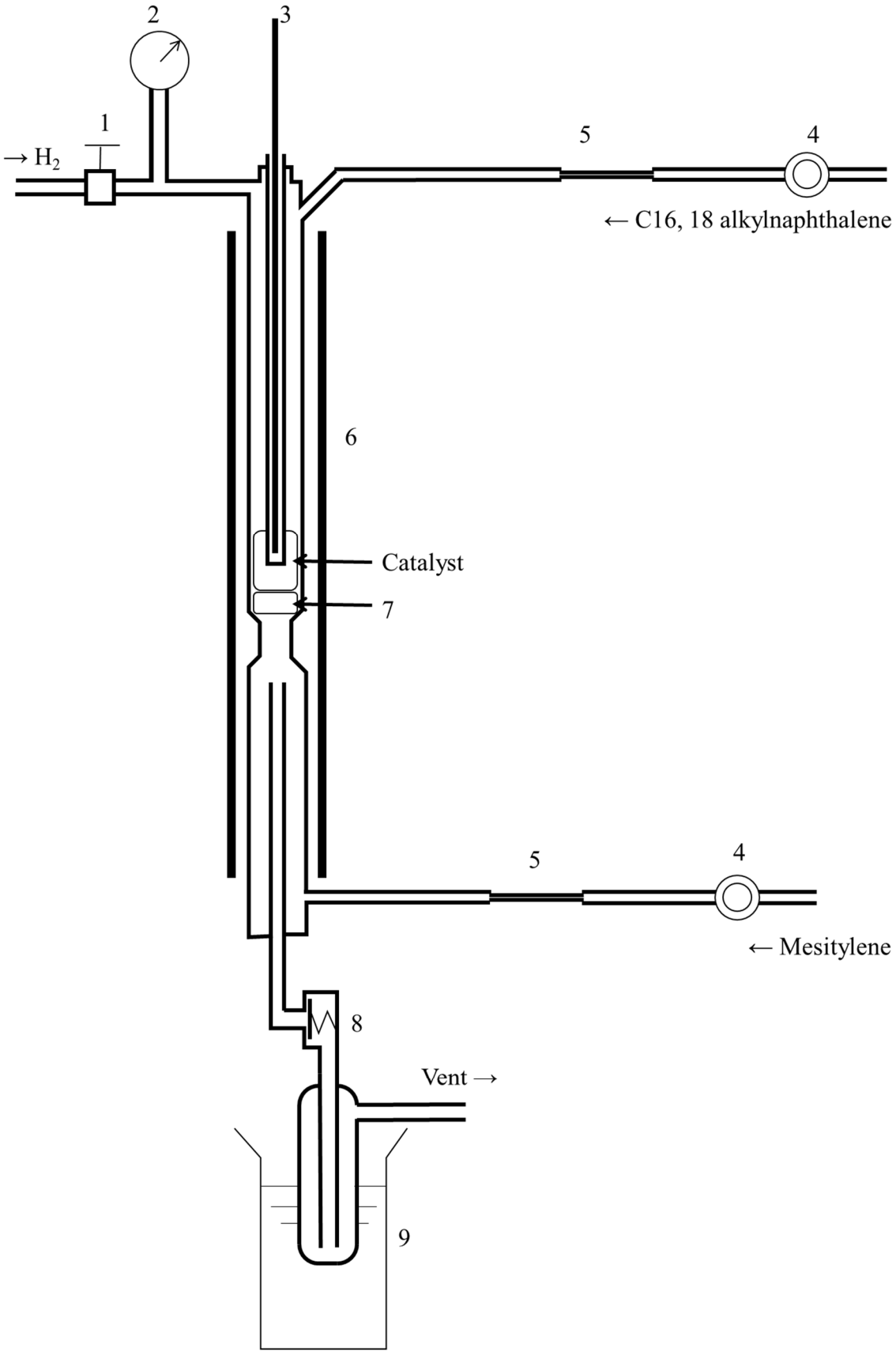
2
3
1
→ H_2
5
4
← C16, 18 alkylnaphthalene
6
Catalyst
7
5
4
← Mesitylene
8
Vent →
9

Figure 2

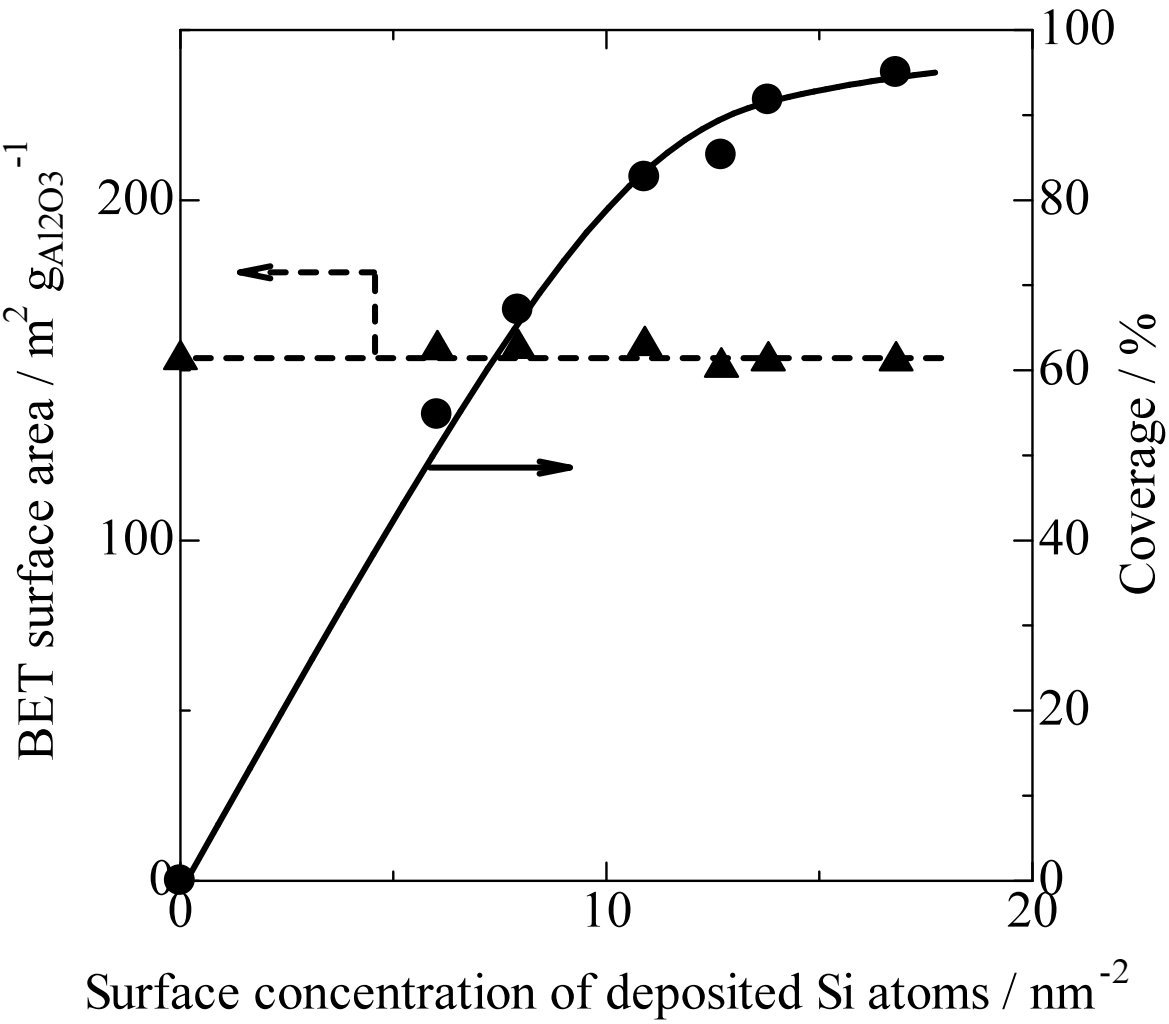
BET surface area / m2 gAl2O3-1
Coverage / %
Surface concentration of deposited Si atoms / nm-2
0
100
200
0
20
40
60
80
100
0
10
20

Figure 3

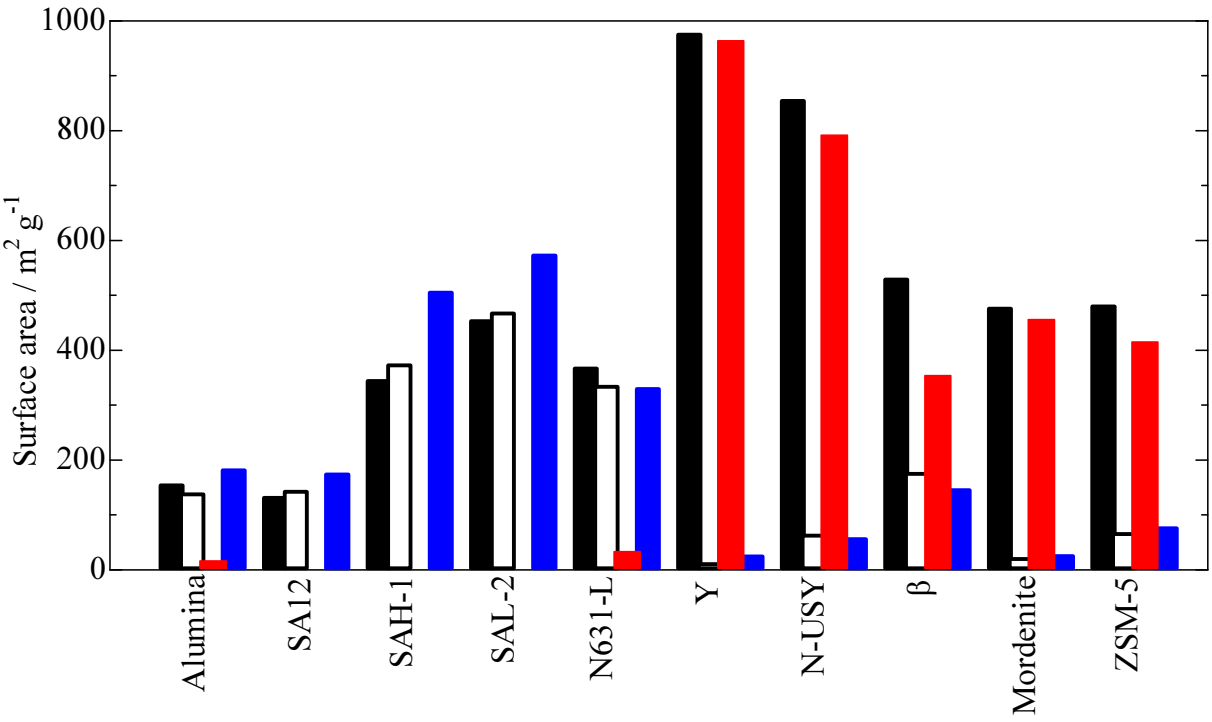
1000
800
600
400
200
0
Surface area / m2 g-1
Alumina
SA12
SAH-1
SAL-2
N631-L
Y
N-USY
β
Mordenite
ZSM-5

Figure 4

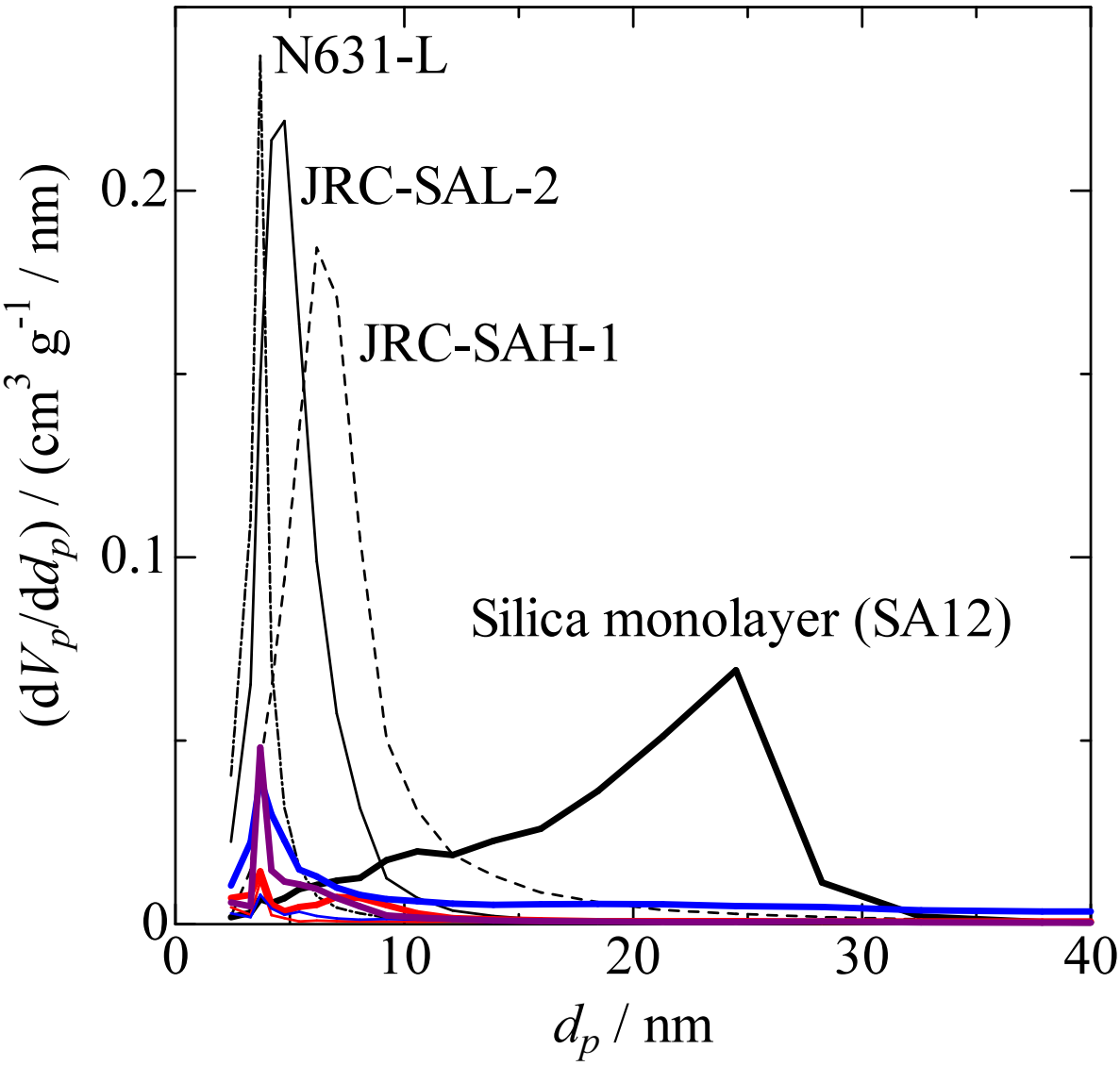
N631-L
JRC-SAL-2
JRC-SAH-1
Silica monolayer (SA12)
0.2
0.1
0
0
10
20
30
40
(dV_p/dd_p) / (cm^3 g^{-1} / nm)
d_p / nm

Figure 5

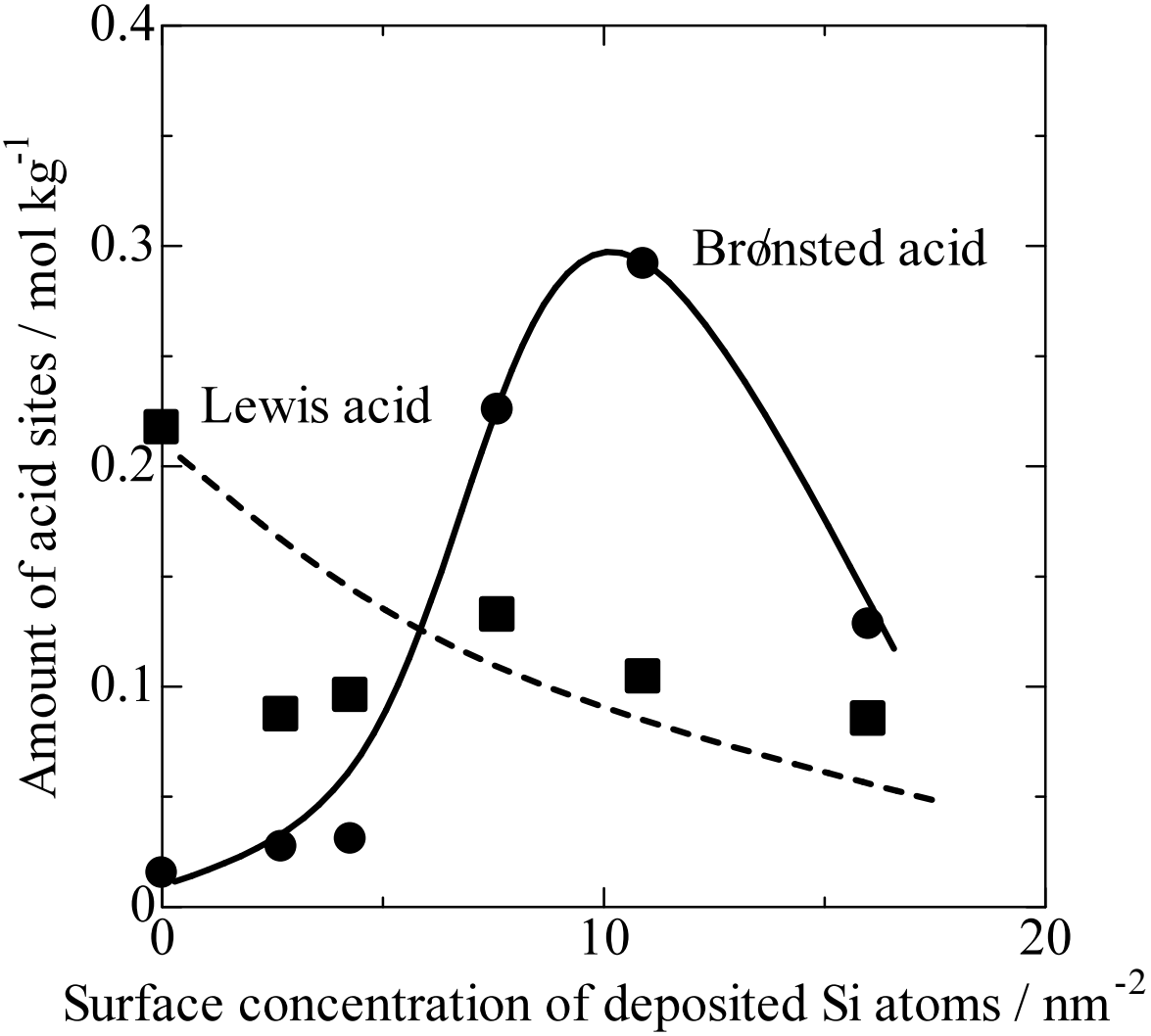
0.4
0.3
0.2
0.1
0
Amount of acid sites / mol kg-1
Brønsted acid
Lewis acid
0
10
20
Surface concentration of deposited Si atoms / nm-2

Figure 6

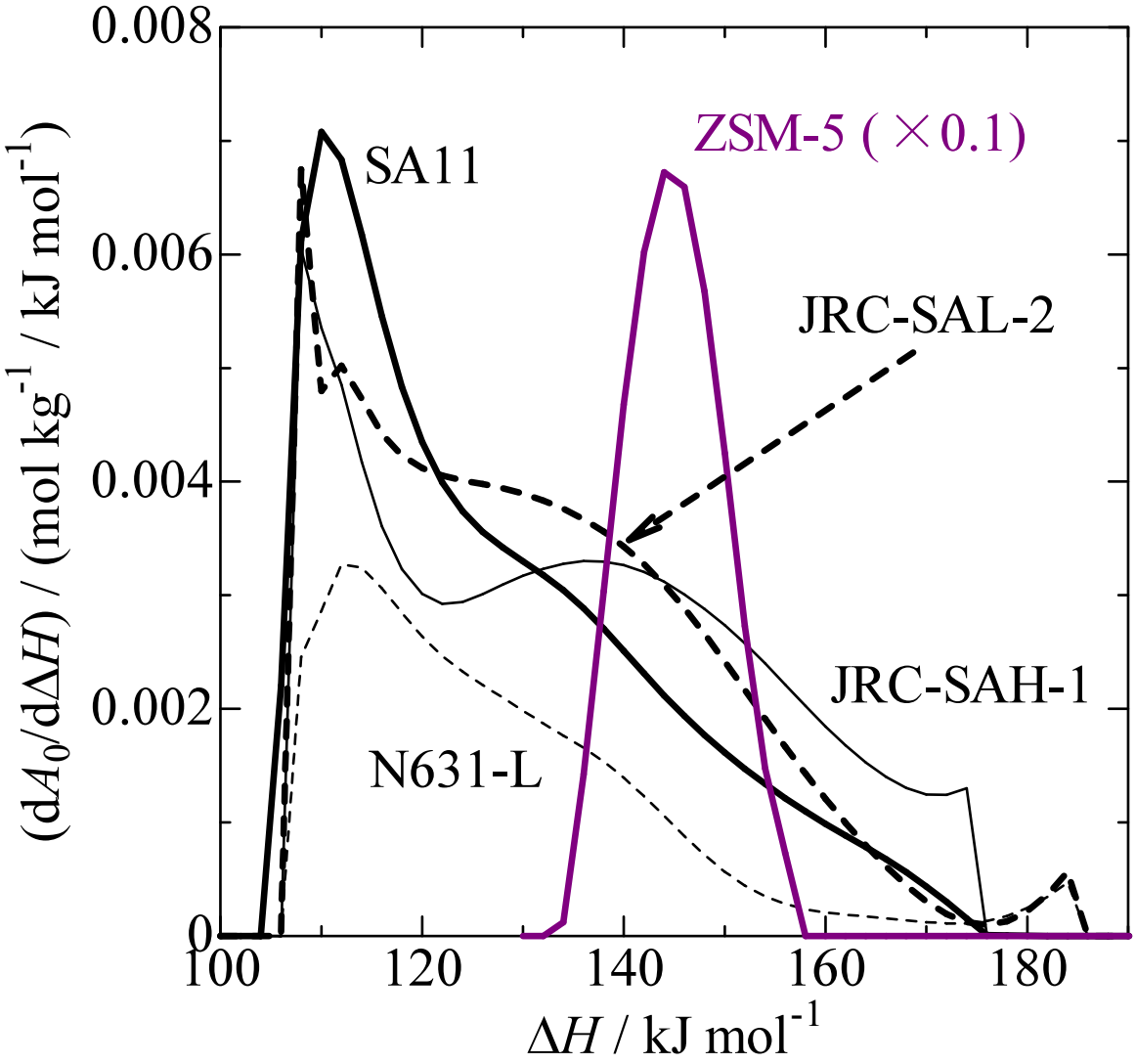
0.008
0.006
0.004
0.002
0
100
120
140
160
180
$(dA_0/d\Delta H)$ / (mol kg^{-1} / kJ mol^{-1})
ΔH / kJ mol^{-1}
SA11
ZSM-5 (×0.1)
JRC-SAL-2
JRC-SAH-1
N631-L

Figure 7

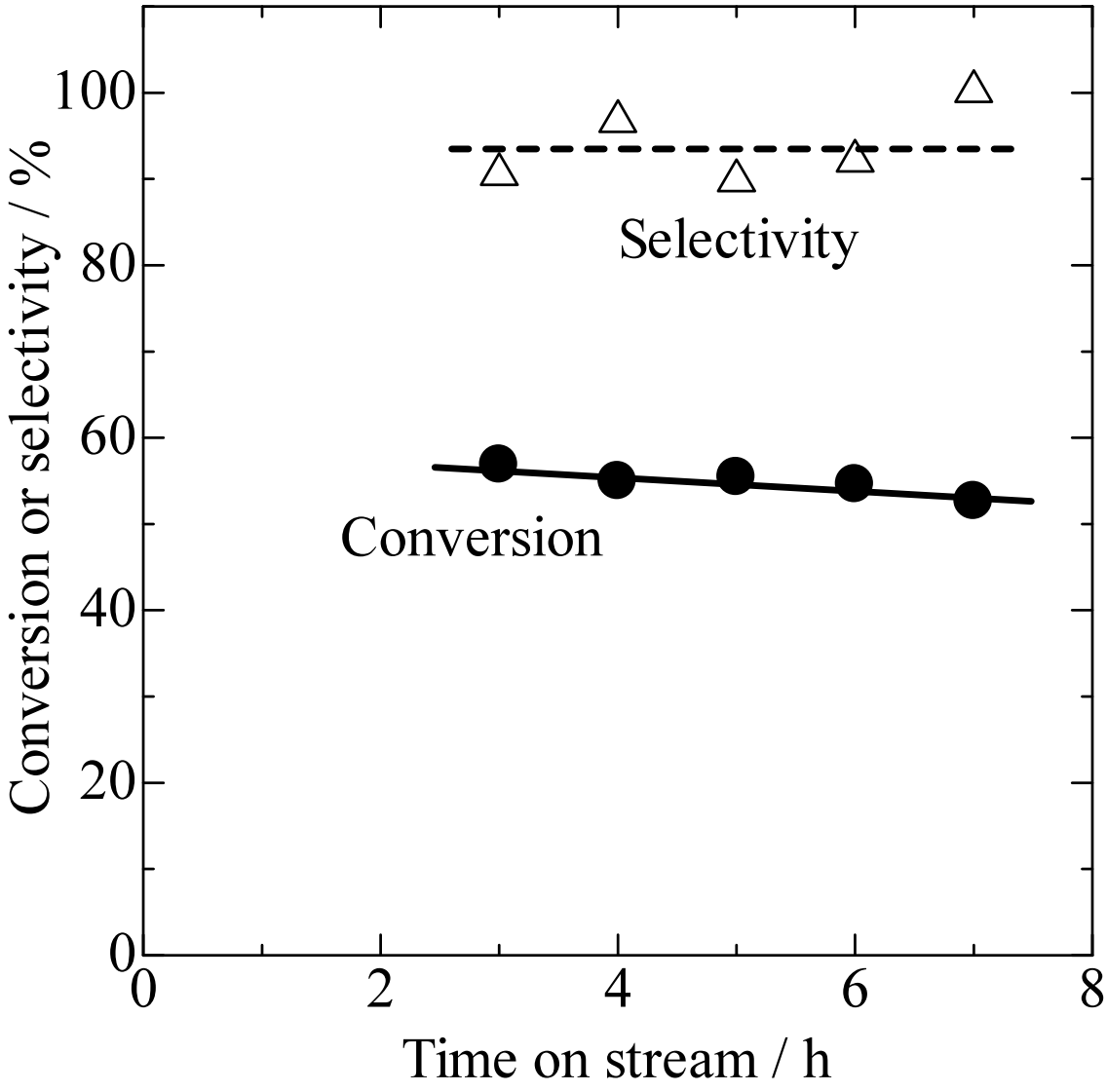
Conversion or selectivity / %
100
80
60
40
20
0
0
2
4
6
8
Time on stream / h
Selectivity
Conversion

Figure 8

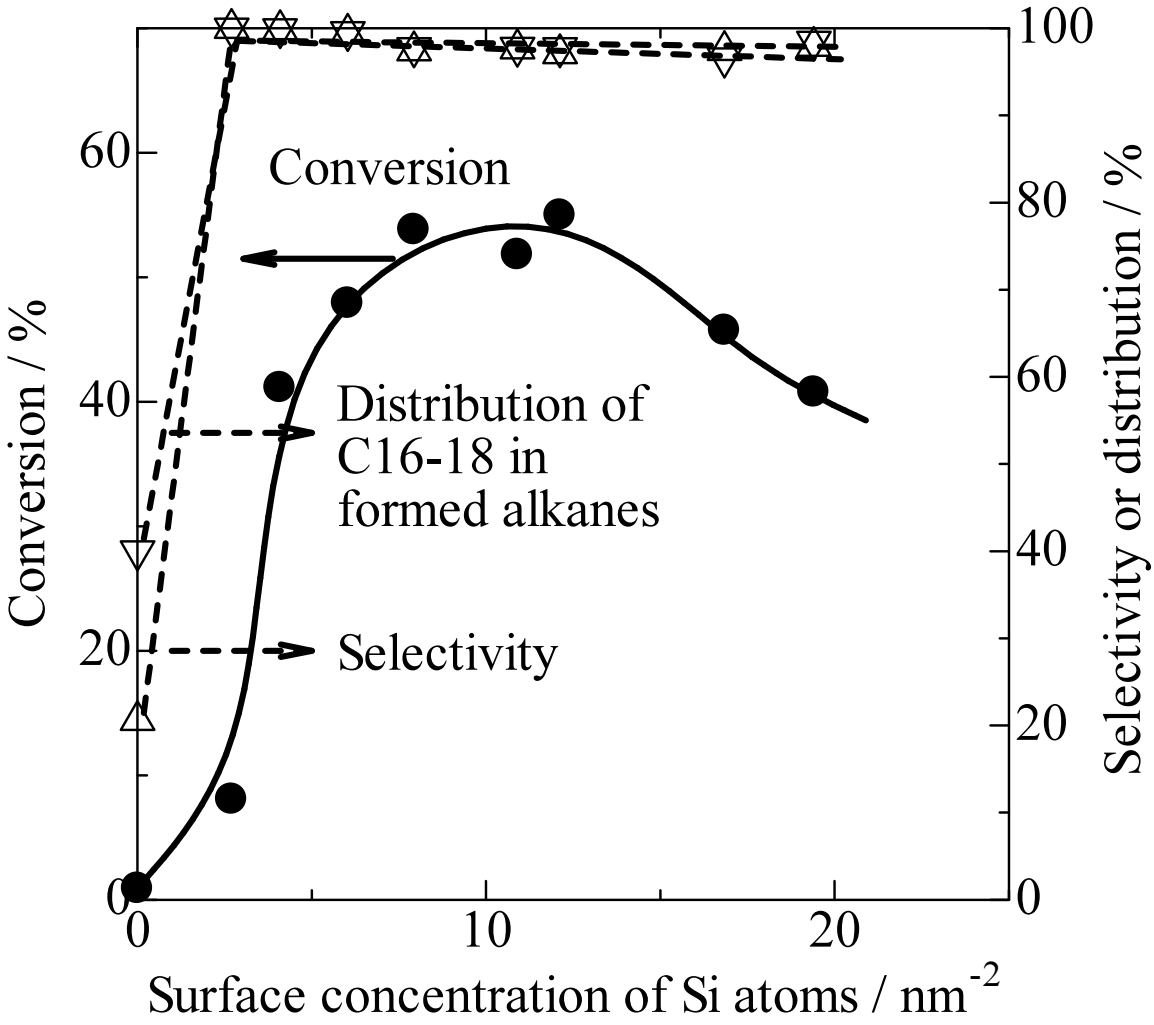
Conversion
Distribution of
C16-18 in
formed alkanes
Selectivity
Conversion / %
Selectivity or distribution / %
Surface concentration of Si atoms / nm-2
0
20
40
60
0
20
40
60
80
100
0
10
20

Figure 9

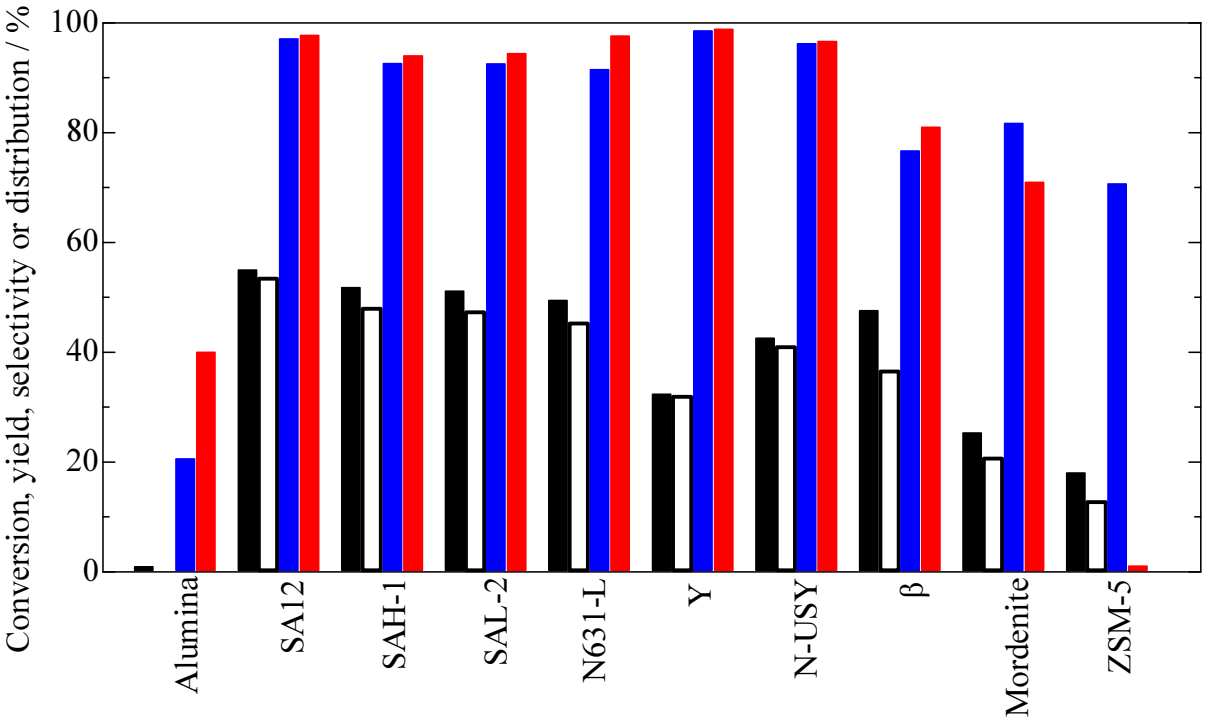
Conversion, yield, selectivity or distribution / %
100
80
60
40
20
0
Alumina
SA12
SAH-1
SAL-2
N631-L
Y
N-USY
β
Mordenite
ZSM-5

Figure 10

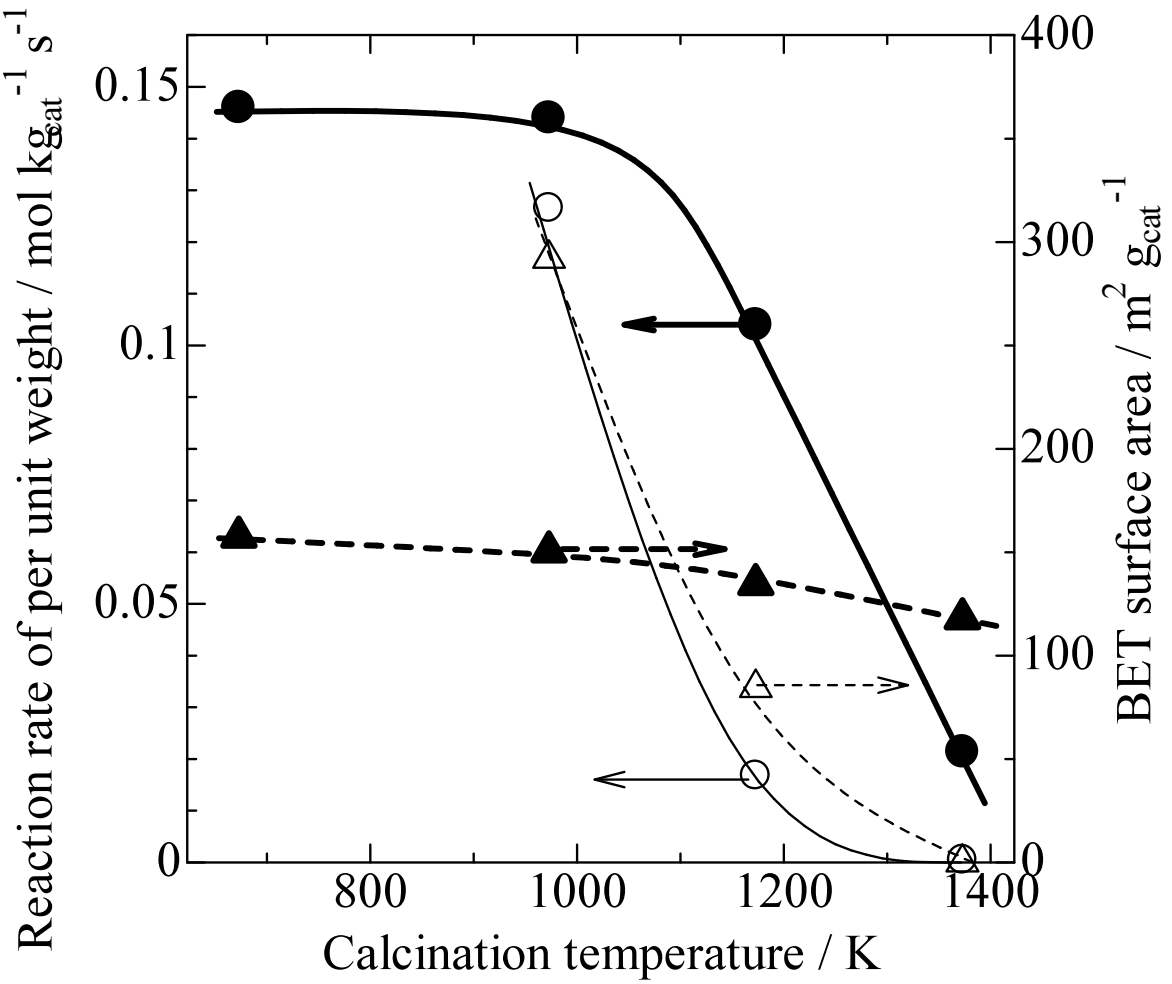
Reaction rate of per unit weight / mol kg$_{cat}^{-1}$ s^{-1}
BET surface area / m^2 g$_{cat}^{-1}$
Calcination temperature / K
0
0.05
0.1
0.15
100
200
300
400
800
1000
1200
1400

Figure 11